Supplemental information

Supplemental Text

Effects of fluorescent protein fragment fusions on Jun ubiquitination. To investigate ubiquitination using UbFC analysis, it is critical that the fluorescent protein fragments do not affect ubiquitination of the substrate being investigated (Baens *et al.*, 2006). To determine if the fluorescent protein fragments fused to Jun and ubiquitin affected Jun ubiquitination, we compared the effects of mutations in Jun and in ubiquitin on the fluorescence intensities of UbFC conjugates with the effects of the same mutations on the levels of ubiquitin conjugates formed by epitope-tagged proteins lacking the fusions. For all mutations in Jun and in ubiquitin, there was a close correspondence between changes in the fluorescence intensities of UbFC conjugates and the levels of ubiquitinated Jun detected by immunoprecipitation and immunoblotting (Figures 1-4). These results indicate that the fluorescent protein fragment fusions did not affect the determinants of Jun ubiquitination in cells.

Ubiquitin and Jun fused to fluorescent protein fragments share many characteristics of the unmodified proteins. Fusion of an intact fluorescent protein to ubiquitin does not inhibit the ubiquitin-proteasome system or endosomal trafficking in cultured cells or transgenic mice (Lindsten *et al.*, 2003; Dantuma *et al.*, 2006). The Jun fusion protein forms heterodimers with Fos and activates transcription of reporter genes containing the AP-1 site (Hu *et al.*, 2002). Jun fused to the fluorescent protein fragment has the same half-life as endogenous Jun in the same cells (Fang and Kerppola, 2004). The UbFC assay therefore enables visualization of ubiquitinated Jun with minimal perturbation of the cell.

Effects of endogenous proteins/ubiquitin on conjugates detected by UbFC and in vitro analysis of the stoichiometry of Jun ubiquitination. The ubiquitin conjugates detected by UbFC as well as in vitro analysis of the stoichiometry of Jun ubiquitination must contain the exogenous fusion proteins, but could also include endogenous proteins associated with these fusions. The bands detected by immunoprecipitation using anti-Xpress antibodies and immunoblotting using anti-HA antibodies could include endogenous cellular proteins as well as the exogenously expressed proteins with the epitope tags. The discrete ladder of bands detected by immunoblotting was shifted by the 3 kDa difference in size between wild type Jun and Jun lacking the δ region, demonstrating that these bands corresponded to ubiquitinated Jun (Figure 1G). The immunoprecipitated conjugates therefore consisted mainly of ubiquitinated Jun rather than interaction partners that could be co-immunoprecipitated with Jun.

The conjugates detected using UbFC or immunoprecipitation and immunoblotting could also contain endogenous ubiquitin. Mixed conjugates containing both endogenous and HA-tagged ubiquitin would have heterogeneous mobilities since the HA-tagged ubiquitin is 1 kDa larger than endogenous ubiquitin. Since discrete bands containing at least 5 ubiquitins are observed, it is unlikely that mixed conjugates constituted a major proportion of the ubiquitinated Jun detected by immunoprecipitation and immunoblotting. The effects of I44A-ubiqutin, K27-only ubiquitin and the co-expression of lysine-less ubiquitin on the stoichiometry of Jun ubiquitination also contradict the interpretation that endogenous ubiquitin accounted for a large proportion of the ubiquitin conjugated to the exogenously expressed Jun. The presence of a large proportion of endogenous ubiquitin in UbFC conjugates formed by the UbI44A and UbK27 ubiquitin mutants is also seemingly inconsistent with the altered localization of these conjugates.

Unless a small proportion of one of these ubiquitin mutants is sufficient to mislocalize the UbFC conjugates, a more parsimonious interpretation is that the small amount of conjugate localized to the cytoplasm reflects the proportion of endogenous ubiquitin in these conjugates.

Polyubiquitination versus multiple mono-ubiquitination of Jun. Since Jun contains 17 lysine residues, we cannot strictly exclude the possibility that it is mono-ubiquitinated at multiple lysine residues. However, the selective effects of UbK27, the level of ubiquitin expression and lysine-less ubiquitin co-expression on specific cycles of ubiquitin conjugation as well as the apparent molecular weight of the largest conjugates (>>188 kDa) are more consistent with poly-ubiquitination. The E3 or E4 ligase(s) that mediate Jun poly-ubiquitination therefore catalyze ubiquitin-K27 isopeptide bond formation.

Concerted effect of ubiquitin variants on the stoichiometry and lysosomal localization of Jun conjugates. The UbFC conjugates produced by UbK27 as well as lysine-less ubiquitin were predominantly nuclear. Co-expression of lysine-less ubiquitin with UbK27 enhanced the lysosomal localization of ubiquitinated Jun. Co-expression of lysine-less ubiquitin with UbK27 reduced the levels of mono- and oligo- ubiquitinated Jun, but did not reduce the level of poly-ubiquitinated Jun (Figure 4G, I). Co-expression of lysine-less ubiquitin had no detectable effect on the ubiquitination of other cellular proteins. We hypothesize that lysine-less ubiquitin selectively inhibited mono-ubiquitination of Jun, but had less effect on extension of the poly-ubiquitin chain. Lysine-less ubiquitin could act as a competitive inhibitor of mono-ubiquitination since it is not effectively conjugated to Jun. Alternatively, it could act as a non-competitive inhibitor by enhancing de-ubiquitination of chains capped by lysine-less ubiquitin,

whereas poly-ubiquitin chains that have escaped lysine-less ubiquitin addition would not be affected.

Effects of the level of Jun expression on UbFC conjugate localization. Under our standard experimental conditions, UbFC conjugates formed by Jun co-localized with LysoTracker Red, EGF-rhodamine, HRS and TSG101 in most, but not all cells. We noticed that cells with higher fluorescence intensities exhibited a lower extent of co-localization between UbFC conjugates formed by Jun and these markers (Figure S4A, data not shown). Under our standard conditions, Jun fused to the fluorescent protein fragment was expressed at an approximately ten fold higher level than endogenous Jun in transfected cells (Figure S4C). Under these conditions, cells with fluorescence intensities 3-10 times higher than average exhibited predominantly cytoplasmic UbFC fluorescence, but the distribution of this fluorescence did not match those of LysoTracker dyes, EGF-rhodamine, HRS or TSG101. Heat shock protein 70 (HSP70) and Itch/AIP4 detected by indirect immunofluorescence co-localized with UbFC conjugates formed by Jun both in cells that exhibited low and high fluorescence intensities (data not shown). Markers of early and late endosomes (EEA1 and MPR respectively) did not co-localize with UbFC conjugates formed by Jun in cells with low or high fluorescence intensities (data not shown). To directly examine the effect of the level of Jun expression on the distribution of UbFC conjugates, we compared the localization of these conjugates in cells transfected with plasmids that expressed different levels of Jun. Overexpression of Jun at a ten-fold higher level resulted in accumulation of UbFC conjugates in the nucleus (Figure S4B, C). Thus, the mechanism controlling the localization of UbFC conjugates was saturable, resulting in lysosomal localization in cells that produced low levels of ubiquitinated Jun,

cytoplasmic localization that did not correspond to lysosomes in cells that expressed intermediate levels, and predominantly nuclear localization in cells that produced high levels of ubiquitinated Jun.

Development of cell lines with reduced HRS and TSG101 levels. To investigate the effects of HRS and TSG101 on the localization of ubiquitinated Jun, we developed cell lines that stably expressed shRNAs complementary to the coding regions of the mRNAs encoding HRS and TSG101. The level of HRS expression was reduced by more than 90% whereas the level of TSG101 expression was reduced by approximately 80% in each line (Figure S5A-C). As a control, a cell line that expressed an shRNA with no complementary sequence in the transcriptome was isolated. To determine the consequences of HRS and TSG101 knockdown on trafficking of the EGF receptor, we examined the distribution of internalized EGF receptor in these cells by incubating them with EGF-rhodamine. Whereas internalized EGF receptor closely matched the distribution of LysoTracker Blue in control cells, it did not co-localize with LysoTracker Blue in HRS or TSG101 knockdown cells (Figure S5D-F). The knockdown of HRS and TSG101 therefore resulted in mis-localization of liganded EGF receptor as predicted based on studies of the EGF receptor trafficking pathway (Bishop *et al.*, 2002; Lu *et al.*, 2003). We compared the distributions of ubiquitinated Jun in HRS and TSG101 knockdown cells with that observed in control cells (Figure 6).

Simulation of the stoichiometry of ubiquitin conjugation. To test the quantitative accuracy of our hypothesis that K27-only ubiquitin selectively affected the conversion of mono- to di-ubiquitinated Jun we developed a simple model of ubiquitination stoichiometry. Based on the amount of mono-ubiquitinated Jun produced, we simulated

the amounts of Jun conjugates with different stoichiometries of ubiquitination in cells that expressed either wild type or K27-only ubiquitin at two different levels of expression. The only variable that was unique for wild type versus K27-only ubiquitin at each level of expression was the efficiency of conversion of mono- to di-ubiquitinated Jun. All other cycles of ubiquitin addition/removal were equivalent for wild type and K27-only ubiquitin at both levels of expression. This simple model reproduced the amounts of di- to hepta-ubiquitinated Jun produced under all conditions with an average error of 10% (Figure S6). The predictive capacity of the model was tested by training the model using the amounts of mono- and di-ubiquitinated Jun produced under all conditions and the amounts of oligo-ubiquitin conjugates produced under a single set of conditions. The model predicted the amounts of the oligo-ubiquitin conjugates produced under all other conditions with an average error of 13-21%. The high predictive capacity of this simple model emphasizes the unique effects of the level of ubiquitin expression and K27-only ubiquitin on mono- and di-ubiquitinated Jun production and the invariance of subsequent cycles of ubiquitin chain extension under the conditions examined.

Supplemental Materials and Methods

Plasmid construction. To construct expression vectors for ubiquitin-mediated fluorescence complementation analysis, the DNA sequence encoding amino acid residues 1-155 of Venus (designated VN) was fused to the 5' end of the coding region for ubiquitin by using an ANSSIDLISVPVEYPYDVPDYASR linker. The chimeric coding region was cloned into the pFlag-CMV2 vector to produce the plasmid encoding VN-Ub. The sequences encoding Jun and Fos were fused to amino acid residues 156-238 of enhanced cyan fluorescent protein (CFP) (designated CC) using a GTRPACKIPNDLKQKVMNH linker. The chimeric coding regions were cloned into the pMyc-CMV vector to produce plasmids encoding Jun-CC and Fos-CC. The sequences encoding Jun, JunB, JunD, FosB, Fra1 and Fra2 were fused to amino acid residues 156-238 of CFP (designated CC) using a GSGGGGSGGGGS linker. The chimeric coding region was cloned into the pEYFP-N3 vector to produce plasmids encoding Jun(HI)-CC, JunB-CC, JunD-CC, FosB-CC, Fra1-CC and Fra2-CC. The plasmids used to express Xpress tagged Jun and hemagglutinin (HA) tagged ubiquitin were described previously (Fang and Kerppola, 2004). The amino acid substitutions in Jun and in ubiquitin were generated by PCR. To construct the plasmid encoding JunYFP, the sequences encoding Jun and YFP were amplified by PCR and inserted between EcoRI/XbaI and XbaI/SmaI sites of plasmid pBiFC-bJunYN155 (Hu *et al.*, 2002). To construct the plasmid encoding UbJunYFP, the sequence encoding ubiquitin was amplified by PCR and inserted between HindIII/EcoRI sites of the plasmid encoding JunYFP. All constructs were confirmed by sequencing the coding regions of the fusion proteins.

Antibodies and fluorescent probes. LysoTracker Blue (L-7525), LysoTracker Red (L-7528), EGF-rhodamine (E-3481), Alexa Fluor 350 donkey anti-goat IgG (A21081) and Alexa Fluor 594 goat anti-mouse IgG (A11032) were from Molecular Probes. Autophagic vacuoles were detected using monodansylcadaverine (MDC; Sigma #30432). The following commercial monoclonal antibodies were used: anti-early endosome antigen-1 (EEA1, sc-6415), Santa Cruz Biotechnology; anti-Mannose 6 Phosphate Receptor (ab2733), Abcam; anti-20S proteasome subunit α5 (pw8270), BIOMOL; anti-TSG101 (sc-7964), Santa Cruz Biotechnology; anti-HRS (ALX-804-382-C050), Alexis; anti-HA (2CA5), Roche; anti-GAPDH (ab9484), Abcam; anti-Xpress (R910-25), Invitrogen. Horseradish peroxidase-conjugated anti-mouse IgG (NAX931) was from GE Healthcare, and Hoechst (B 1155) was purchased from Sigma.

Cell culture and transfection. Except where stated, all experiments were performed using COS-7 cells. The cells were maintained in Dulbecco's modified Eagle medium (GIBCO) supplemented with 10% fetal bovine serum and antibiotics at 37^{o}C in 5% CO_2. For transfection, the cells were plated at a density of 1 x 10^5 cells/well in 6-well plates (140675, Nalge Nunc International) or 5 x 10^4 cells/well in 2-well cover glass chambers (155379, Nalge Nunc International) or 6 x 10^5 cells/plate in 100-mm plates (430167, Corning) . 24 hours after plating, a total of 1, 0.5 or 6 μg of DNA was transfected in each well of a 6-well plate, a 2-well cover glass chamber or a 100-mm plate, respectively. Fugene 6 (Roche) was used for all transfection.

Quantitative comparison of the distributions of UbFC conjugates. Cells were grown in cover glass chambers (155379, Nalge Nunc International) for live cell imaging or on cover glass (12-541B, Fisherbrand) in 6-well plates for analysis of fixed cells. Plasmids

encoding the proteins indicated in each experiment were co-transfected into cells 24 hours after plating. BiFC fluorescence was imaged 20-24 hours after transfection. To image fixed cells, cells grown on cover glass were fixed and mounted on microscope slides. Nuclei were labeled by incubation of the cells with Hoechst for 3 minutes prior to imaging or fixation. The fluorescence images were acquired using a Nikon TE300 inverted fluorescence microscope with a Hamamatsu Orca ER charge-coupled device camera. Both YFP and UbFC fluorescence were measured by excitation at 500 nm and emission at 535 nm. UbFC images were recorded using a 4 second exposure time. JunYFP and UbJunYFP signals were recorded using a 1 second exposure time. The fluorescence intensities of the nucleus and cytoplasm of individual cells were quantified using SimplePCI software.

Analysis of UbFC conjugate localization by immunofluorescence and fluorescent dye labeling. For immunofluorescence analysis, transfected cells grown on cover glass were fixed in 3.7% paraformaldehyde in PBS, and permeabilized with 0.5% Triton X-100. The samples were blocked in 5% bovine serum albumin in PBS for 30 min and incubated with anti-EEA1 (1:20), anti-Mannose 6 Phosphate Receptor (1:100), anti-20S proteasome subunit α5 (1:20), anti-TSG101 (1:20) or anti-HRS antibody (1:50) in PBS containing 1% BSA for 1 h. The immune complexes were visualized using Alexa Fluor 350 donkey anti-goat IgG (1:200) or Alexa Fluor 594 goat anti-mouse IgG (1:500). The samples were washed using PBS containing 10 μg/ml Hoechst and mounted on microscope slides. For fluorescent dye labeling, transfected cells cultured in cover glass chambers were incubated with the dyes indicated for 30 or 60 min at 37°C. LysoTracker dyes were used at a final concentration of 50 nM. For EGF-rhodamine labeling, the cells were incubated

with 100 ng/ml EGF-rhodamine in DMEM medium on ice for 1 h, transferred into medium at 37 °C and incubated an additional 30 or 60 minutes (Chen *et al.*, 1998). The cells were washed twice with medium to remove excess dyes, and rinsed with medium containing 10 μg/ml Hoechst before imaging.

Preparation of images for presentation. All images were cropped to 38.5 μm x 38.5 μm size for presentation. The background signal in an area of the image outside the cell was subtracted from all pixels in the image. No other contrast adjustments of the UbFC fluorescence were performed. Immunofluorescence and fluorescent label images were adjusted to show maximal dynamic range. The images were false-colored by substituting green or red for the grayscale values and were superimposed using Adobe Photoshop CS2 software.

Immunoprecipitation and Immunoblotting. COS-1 cells transfected with the indicated plasmids were harvested 36 h after transfection and the cells were extracted using NP-40 lysis buffer (20 mM Tris-HCl, pH 7.5, 150 mM NaCl, 5 mM EDTA, pH 8, 1% NP-40, 1mM $NaVO_4$, 1 mM PMSF, protease inhibitor cocktail - Roche). For immunoprecipitation, the extracts were precleared using 30 μl protein G agarose beads (Upstate) and 30 μg bovine serum albumin for 1h at 4° C. The precleared cell extracts were incubated with anti-Xpress for 1 h at 4° C, and were added to 40 μl of protein G agarose beads. After 1 h incubation, the agarose beads were washed 4 times with NP-40 lysis buffer and boiled in SDS sample buffer. For immunoblot analysis, the proteins were separated by SDS-PAGE and transferred to Immobilon-P membrane (Millipore). The membrane was blocked in 5% skim milk/PBST (0.05% Tween 20 in PBS) and incubated with primary antibody using anti-HA (1:1000), anti-Xpress (1:5000), anti-Jun (1:1000),

anti-TSG101 (1:300), anti-HRS (1:1000) or anti-GAPDH (1:5000) for 1 h, followed by secondary antibody for 1 h. The primary and secondary antibodies were diluted in 3% skim milk/PBST. The immunoreactive bands were detected using ECL (GE Healthcare). Band intensities were measured using NIH Image J software.

RNA interference by shRNA expression. Plasmids for the expression of shRNA directed against HRS and TSG101 were constructed by insertion of oligonucleotides encoding RNA harpins with a 19 base pair stem and a 9 nucleotide loop (Brummelkamp *et al.*, 2002) into the pSUPER.puro plasmid (OligoEngine). At least three constructs expressing different shRNA sequences were generated for each target RNA and the constructs that demonstrated the greatest effectiveness in decreasing the levels of the target proteins were used. The sequences of the stems of successful constructs targeting TSG101 and HRS were 5'-GCCTACTAGTTCAATGACT-3' and 5'- GTACAAGGTGGTCCAGGAC-3', respectively. A sequence with no complementary target in the transcriptome 5'-GATCCGTAGTCGTACGAGC-3' was used as a control. To generate stable cell lines expressing the shRNAs, COS-7 cells were transfected with 1μg of the shRNA constructs and cultured 14 days in the presence of 1 μg/ml puromycin. Cell colonies were picked, expanded, and analyzed for TSG101 or HRS protein levels by immunoblotting. For rescue experiments, expression vectors encoding mouse TSG101 or HRS that do not contain the sequences targeted by the shRNAs were transfected into each knockdown cell line. Plasmids pLLmHRS and pLLTSG101 encoding wild-type HRS and TSG101 were generously provided by Dr. Stanley Cohen.

Analysis of Jun degradation. To analyze the degradation of transient transfected Jun, cells were plated at a density of 6×10^5 cells/100-mm plate and transfected with 3 μg of

a plasmid encoding Xpress-tagged Jun and 3 μg pcDNA3.1. Ten hours after transfection, the cells were split at a density of 8 x 10^4 cells/well in 6-well plates. 24 hours after the split, 50 μg/ml cycloheximide (CHX) was added, and the cells were incubated for the times indicated. The cells were harvested and the cell lysates were analyzed by immunoblotting using anti-Xpress antibody. To analyze the degradation of endogenous Jun, cells were plated at a density of 8 x 10^4 cells/well in 6-well plates, treated with cycloheximize and analyzed as described above.

Supplemental References

Baens, M., Noels, H., Broeckx, V., Hagens, S., Fevery, S., Billiau, A.D., Vankelecom, H., and Marynen, P. (2006). The dark side of EGFP: defective polyubiquitination. PLoS ONE *1*, e54.

Bishop, N., Horman, A., and Woodman, P. (2002). Mammalian class E vps proteins recognize ubiquitin and act in the removal of endosomal protein-ubiquitin conjugates. The Journal of cell biology *157*, 91-101.

Brummelkamp, T.R., Bernards, R., and Agami, R. (2002). A system for stable expression of short interfering RNAs in mammalian cells. Science (New York, N.Y *296*, 550-553.

Chen, H., Fre, S., Slepnev, V.I., Capua, M.R., Takei, K., Butler, M.H., Di Fiore, P.P., and De Camilli, P. (1998). Epsin is an EH-domain-binding protein implicated in clathrin-mediated endocytosis. Nature *394*, 793-797.

Dantuma, N.P., Groothuis, T.A., Salomons, F.A., and Neefjes, J. (2006). A dynamic ubiquitin equilibrium couples proteasomal activity to chromatin remodeling. The Journal of cell biology *173*, 19-26.

Fang, D., and Kerppola, T.K. (2004). Ubiquitin-mediated fluorescence complementation reveals that Jun ubiquitinated by Itch/AIP4 is localized to lysosomes. Proc Natl Acad Sci U S A *101*, 14782-14787.

Hu, C.D., Chinenov, Y., and Kerppola, T.K. (2002). Visualization of interactions among bZIP and Rel family proteins in living cells using bimolecular fluorescence complementation. Molecular cell *9*, 789-798.

Lindsten, K., Menendez-Benito, V., Masucci, M.G., and Dantuma, N.P. (2003). A transgenic mouse model of the ubiquitin/proteasome system. Nature biotechnology *21*, 897-902.

Lu, Q., Hope, L.W., Brasch, M., Reinhard, C., and Cohen, S.N. (2003). TSG101 interaction with HRS mediates endosomal trafficking and receptor down-regulation. Proc Natl Acad Sci U S A *100*, 7626-7631.

Supplemental Table

Table S1. Stoichiometries of Jun ubiquitination by different ubiquitin variants [1]

	Ub	Ub x2	UbK27	UbK27 x2	UbnoK	UbnoK x2	UbK27 + UbnoK
Ub1	**45 (5)**	**127 (7)**	**89 (43)**	**207 (51)**	**8 (16)**	**4 (9)**	**4 (5)**
↓	3.6	2.2	0.2	0.1			
Ub2	**160 (16)**	**277 (15)**	**14 (7)**	**23 (6)**	**6 (11)**	**4 (10)**	**3 (4)**
↓	1.1	1.1	1.8	1.6			
Ub3	**184 (18)**	**310 (16)**	**25 (12)**	**37 (9)**	**7 (13)**	**7 (16)**	**8 (10)**
↓	1.1	1.1	0.8	0.8			
Ub4	**194 (19)**	**333 (18)**	**19 (9)**	**28 (7)**	**7 (12)**	**6 (14)**	**8 (9)**
↓	0.7	0.9	0.8	0.9			
Ub5	**141 (14)**	**287 (15)**	**15 (7)**	**26 (6)**	**7 (13)**	**6 (13)**	**9 (11)**
↓	0.7	0.6	0.8	1.0			
Ub6	**95 (9)**	**186 (10)**	**12 (6)**	**25 (6)**	**5 (10)**	**5 (11)**	**9 (11)**
↓	0.8	0.7	0.8	0.9			
Ub7	**77 (8)**	**132 (7)**	**10 (5)**	**21 (5)**	**5 (10)**	**5 (10)**	**9 (11)**
↓↓↓	1.3	1.9	2.5	2.0			
Ub8+	**104 (10)**	**249 (13)**	**25 (12)**	**43 (11)**	**8 (15)**	**8 (18)**	**32 (39)**
Total	**1000 (100)**	**1902 (100)**	**209 (100)**	**411 (100)**	**53 (100)**	**44 (100)**	**81 (100)**

[1] The values in boldface show the relative intensities of bands corresponding to conjugates formed by the ubiquitin variants indicated in the top row with the stoichiometries of ubiquitination indicated in the left column. The intensity of each band is expressed relative to the total intensity of bands produced by one equivalent of wild type ubiquitin set to 1000. The percentage represented by each band of the total formed by the ubiquitin variant(s) tested is listed in parenthesis. The ratio between bands that

differ by the addition or removal of one ubiquitin is shown in the rows indicated by arrows in the left column. The intensities of most bands formed by UbnoK alone or in combination with UbK27 were too low (<10) to calculate meaningful ratios. Note that conjugates with different stoichiometries of ubiquitin contained different numbers of HA epitopes. The relationship between the ECL signal and the number of epitopes on the same conjugate is not known. Therefore the absolute levels can only be compared between conjugates that have the same stoichiometry of ubiquitination. The band intensities were measured by scanning a non-saturated exposure of the autoradiogram shown in Figure 4G and quantified using ImageJ. Scans of multiple exposures were compared to ensure that the relative band intensities were not affected by the exposure time. The data are representative of at least three independent experiments for each ubiquitin variant, and the concentration-dependence was established based on comparison of three different ubiquitin variants in the same experiment.

Figure S1

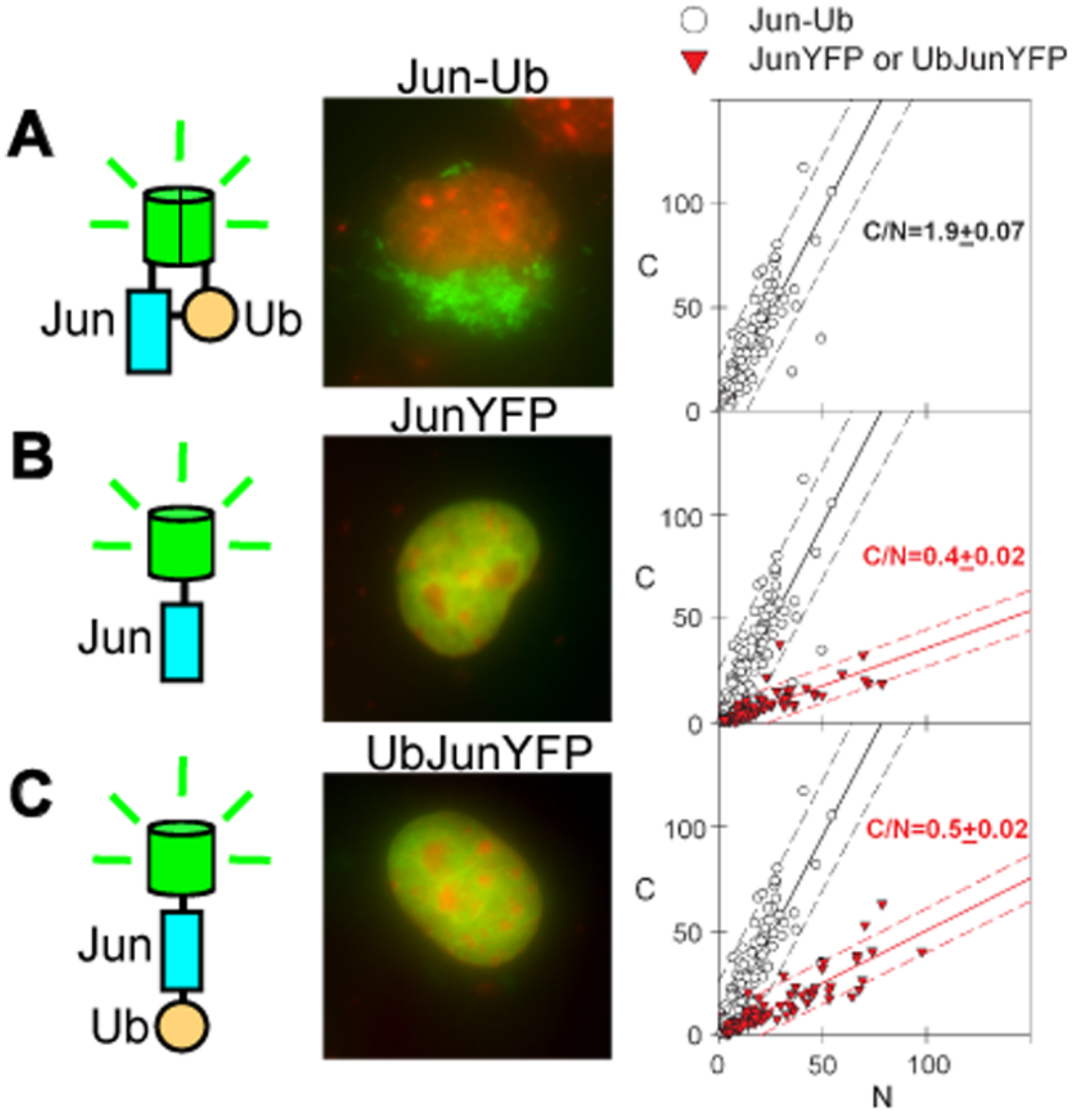
A
Jun
Ub
Jun-Ub
B
Jun
JunYFP
C
Jun
Ub
UbJunYFP
Jun-Ub
JunYFP or UbJunYFP
C/N=1.9±0.07
C/N=0.4±0.02
C/N=0.5±0.02
C
N
0
50
100

Figure S1. Distinct effects of the conjugation and fusion of ubiquitin to Jun. The distributions of UbFC conjugates **A** and fusions to intact YFP **B, C** were visualized by fluorescence imaging. The fluorescence of the UbFC conjugates and intact fluorescent proteins (green) was superimposed with Hoechst staining of DNA (red). The diagrams to the left of the images depict the proteins expressed in each cell (Jun-blue, ubiquitin-orange, fluorescent proteins or fragments-green). The fluorescence intensities of the cytoplasm (C) and nucleus (N) were measured in individual cells and plotted using red triangles in a scatterplot (graphs to the right). Data for UbFC conjugates of Jun analyzed in parallel were plotted as a reference in each graph using open circles. The best linear fit to the data is shown as a solid line and the 95% confidence interval is shown as dashed lines. Each plot is representative of at least three independent experiments.

Figure S2

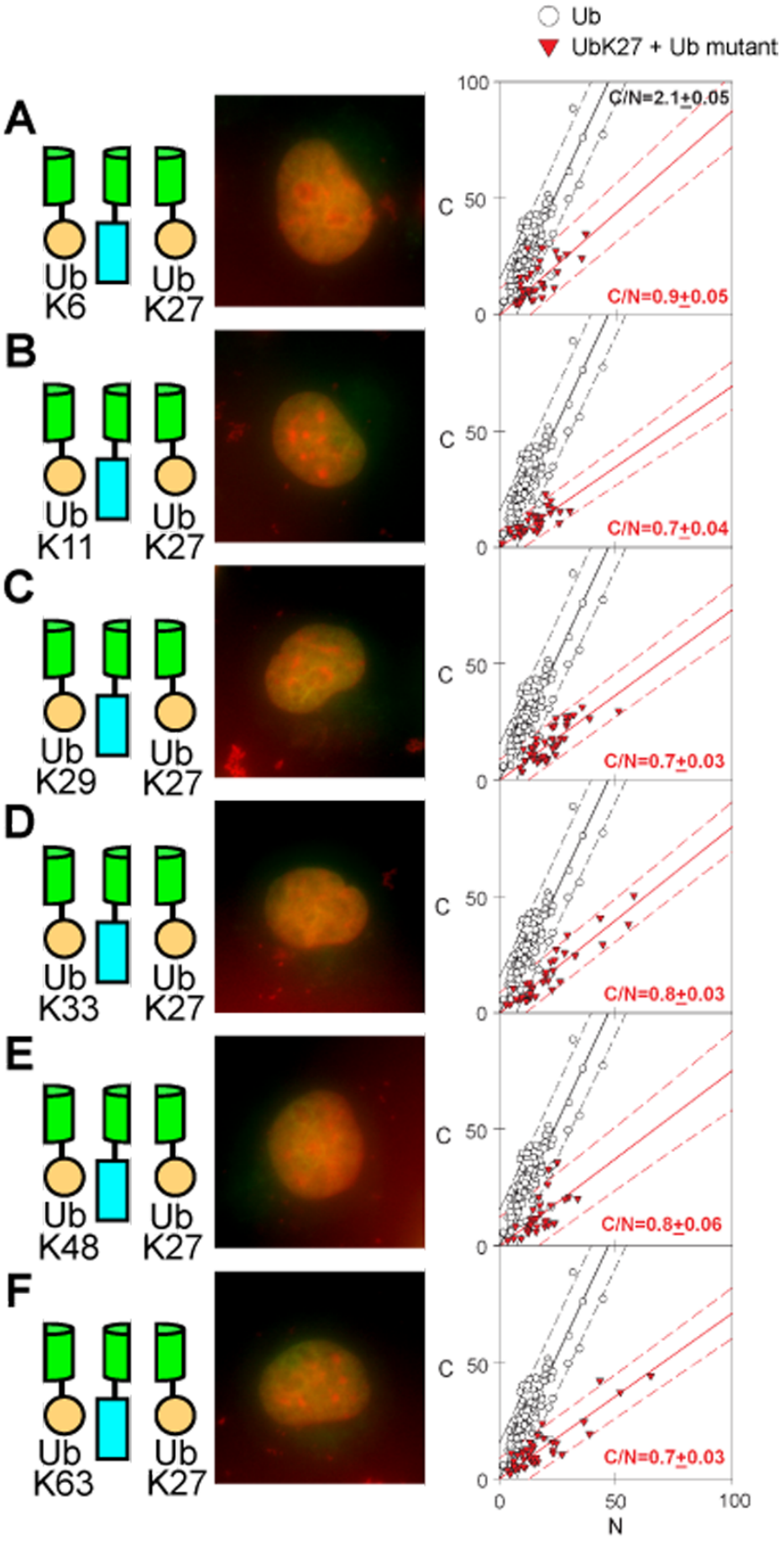
Ub
UbK27 + Ub mutant
A
Ub K6
Ub K27
B
Ub K11
Ub K27
C
Ub K29
Ub K27
D
Ub K33
Ub K27
E
Ub K48
Ub K27
F
Ub K63
Ub K27
C/N=2.1±0.05
C/N=0.9±0.05
C/N=0.7±0.04
C/N=0.7±0.03
C/N=0.8±0.03
C/N=0.8±0.06
C/N=0.7±0.03
C
N
0
50
100

Figure S2. Localization of Jun conjugated to single-lysine ubiquitin mutants. A-F The distributions of conjugates formed by Jun and the ubiquitin mutants indicated in each panel were visualized using UbFC analysis (green). The images were superimposed with Hoechst staining of DNA (red). The diagrams to the left of the images depict the proteins expressed in the cells (Jun-blue, ubiquitin-orange, fluorescent proteins or fragments-green). The fluorescence intensities of the cytoplasm (C) and nucleus (N) were measured in individual cells and plotted as a scatterplot (graphs to the right of images). Data for each ubiquitin mutant are shown using red triangles and the data for wild-type ubiquitin obtained in a parallel experiment are shown using open circles. The best linear fit to data is shown as a solid line and the 95% confidence interval is shown as dashed lines. .

Figure S3

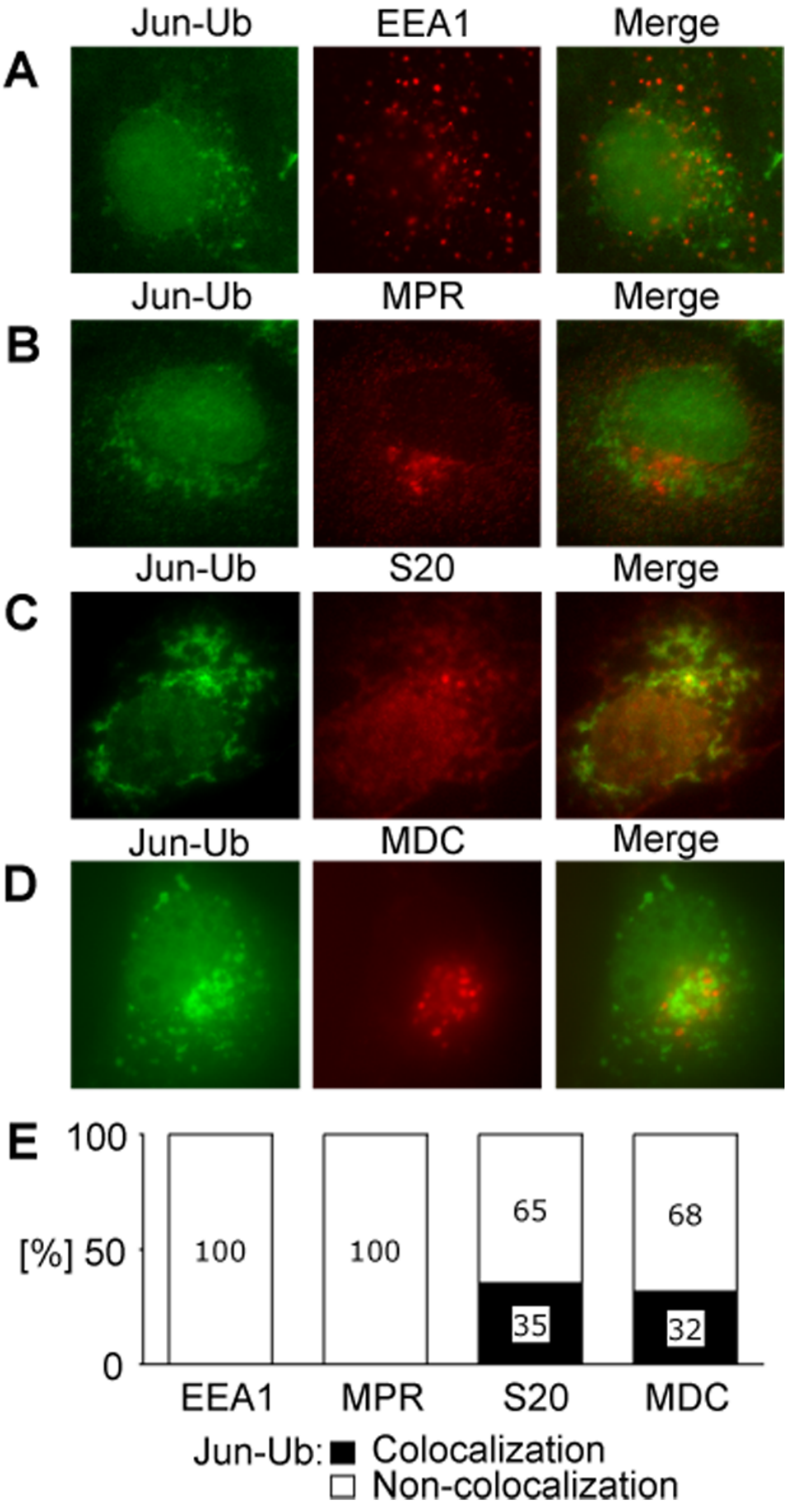
Jun-Ub
EEA1
Merge
A
Jun-Ub
MPR
Merge
B
Jun-Ub
S20
Merge
C
Jun-Ub
MDC
Merge
D
E
100
[%] 50
0
100
100
65
35
68
32
EEA1
MPR
S20
MDC
Jun-Ub: Colocalization
Non-colocalization

Figure S3. Localization of ubiquitinated Jun compared with sites of protein folding and degradation. The distribution of ubiquitinated Jun visualized using UbFC analysis (left - green) was compared with **A** anti-early endosome antigen-1 (EEA1), **B** anti-mannose 6-phosphate receptor (MPR), **C** anti-proteasome S20 subunit (S20) immunostaining in fixed cells as well as **D** monodansyl-cadaverine (MDC) labeling of live cells (center - red). The images were superimposed to produce merged images (right). **E** The percentage of cells in which more than half of the UbFC fluorescence overlapped with the markers indicated was plotted as a histogram.

Figure S4

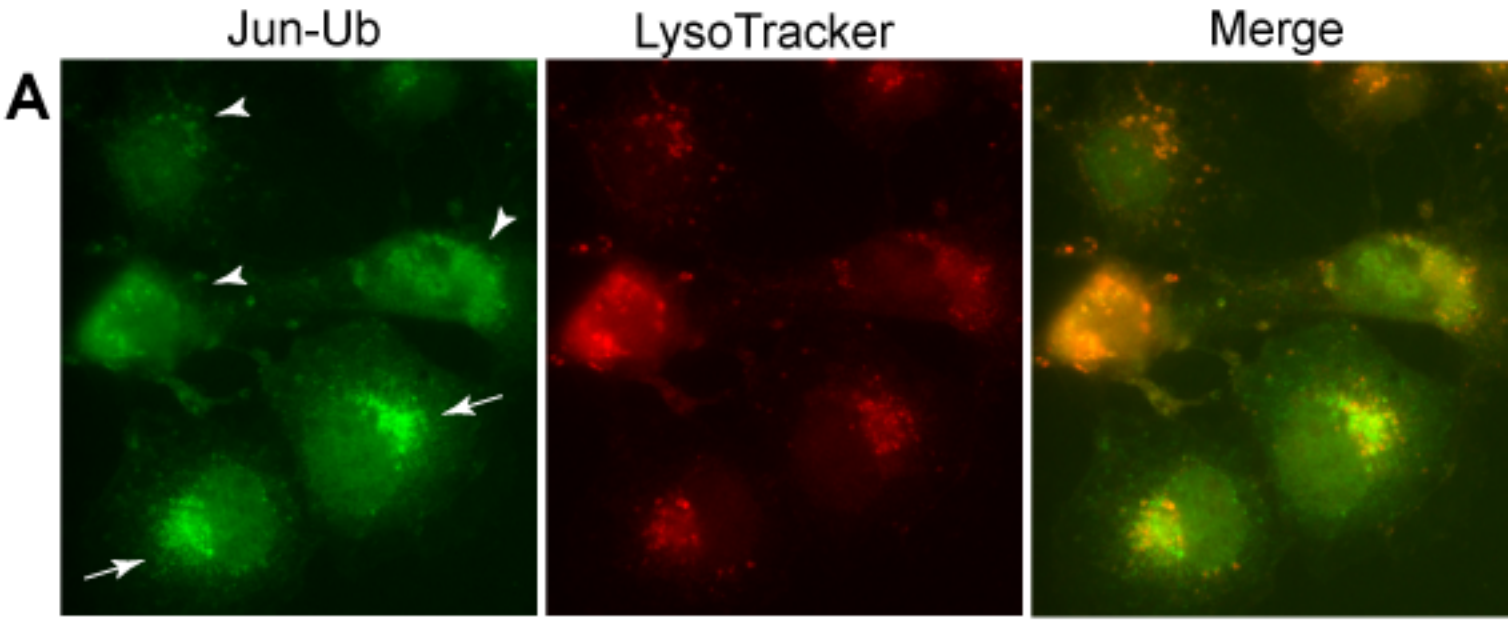
A
Jun-Ub
LysoTracker
Merge

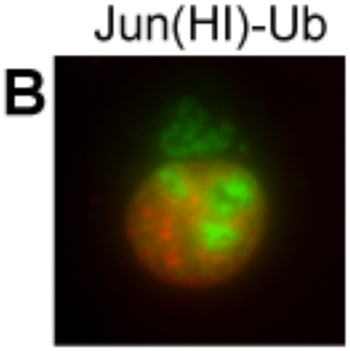
B
Jun(HI)-Ub

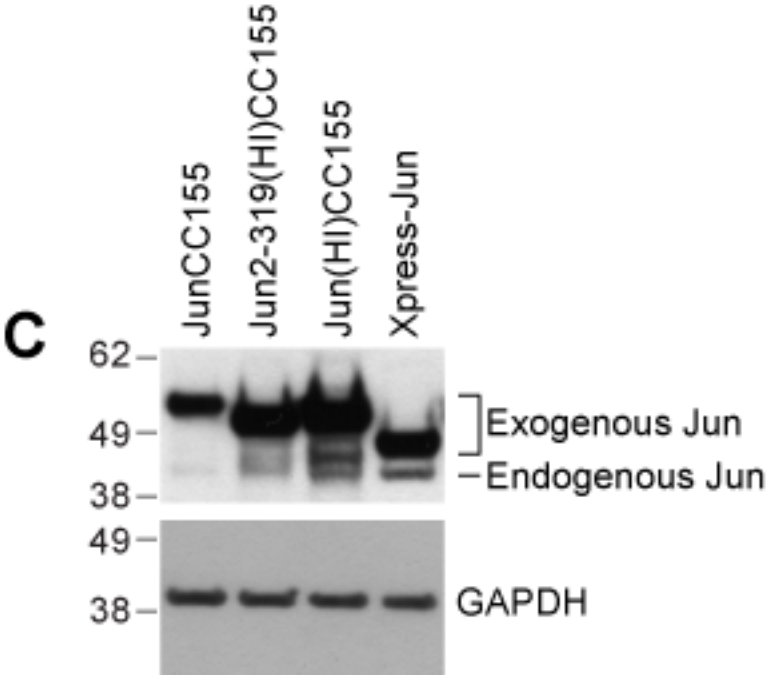
C
JunCC155
Jun2-319(HI)CC155
Jun(HI)CC155
Xpress-Jun
62
49
38
Exogenous Jun
Endogenous Jun
49
38
GAPDH

Figure S4. Localization of ubiquitinated Jun in cells overexpressing Jun. A The distribution of ubiquitinated Jun was visualized by UbFC analysis in cells that containined different levels of UbFC conjugates. Cells that had lower UbFC fluorescence intensities (arrowheads) displayed close co-localization of ubiquitinated Jun and LysoTracker Red. Cells with high intensity UbFC fluorescence (arrow) displayed less co-localization of ubiquitinated Jun and LysoTracker Red. **B** The distribution of ubiquitinated Jun was visualized by UbFC analysis (green) of cells that overexpressed Jun at ten-fold higher levels. The UbFC fluorescence was superimposed on Hoechst staining of DNA (red). **C** Endogenous and exogenous Jun's expression level. JunCC155, Jun(HI)CC155, Jun2-319 a.a (HI)CC155 and Xpress-tagged Jun were transfected into cells. Twenty-four hours after the transfection, cells were harvested and analyzed by immunoblotting using anti-Jun antibody. The same membrane was reblotted using anti-GAPDH antibody.

Figure S5

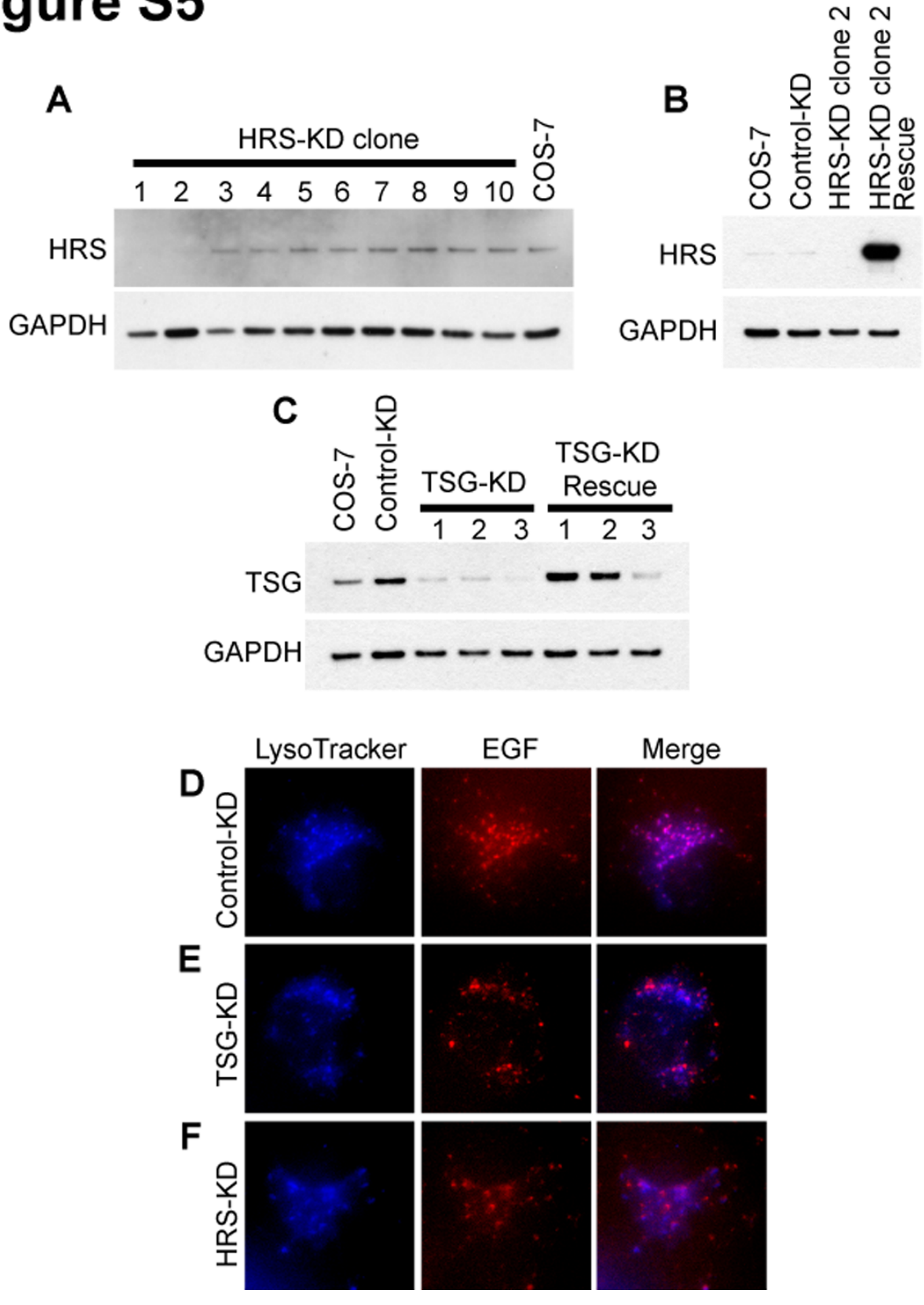
A
HRS-KD clone
1 2 3 4 5 6 7 8 9 10
COS-7
HRS
GAPDH
B
COS-7
Control-KD
HRS-KD clone 2
HRS-KD clone 2 Rescue
HRS
GAPDH
C
COS-7
Control-KD
TSG-KD
TSG-KD Rescue
1 2 3 1 2 3
TSG
GAPDH
LysoTracker
EGF
Merge
D
Control-KD
E
TSG-KD
F
HRS-KD

Figure S5. Development of HRS and TSG101 knockdown cells. A,B Immunoblot analysis of the levels of HRS expression in COS-7 cells, cells that expressed an shRNA with no complementary sequence in the genome (Control-KD), cells that expressed an shRNA complementary to HRS (HRS-KD), and the former cells transfected with a plasmid encoding an shRNA-resistant HRS transcript (HRS-KD Rescue). The membrane was re-blotted using anti-GAPDH antibody to determine the levels of protein loaded. **C** Immunoblot analysis of the levels of TSG101 expression in COS-7 cells, cells that expressed an shRNA with no complementary sequence in the genome (Control-KD), three cell lines that expressed an shRNA complementary to TSG101 (TSG-KD), and the former cells transfected with a plasmid encoding an shRNA-resistant TSG101 transcript (TSG-KD Rescue). The membrane was re-blotted using anti-GAPDH antibody to determine the levels of protein loaded. **D-F** Comparison of EGF receptor localization in Control-KD, HRS-KD and TSG-KD cells. Cells incubated with LysoTracker Blue (LysoTracker - left - blue) and EGF-rhodamine (EGF - center - red) were imaged using 373 nm excitation and 422 nm emission as well as 555 nm excitation and 580 nm emission wavelengths respectively. The images were superimposed to produce merged images (right).

Figure S6

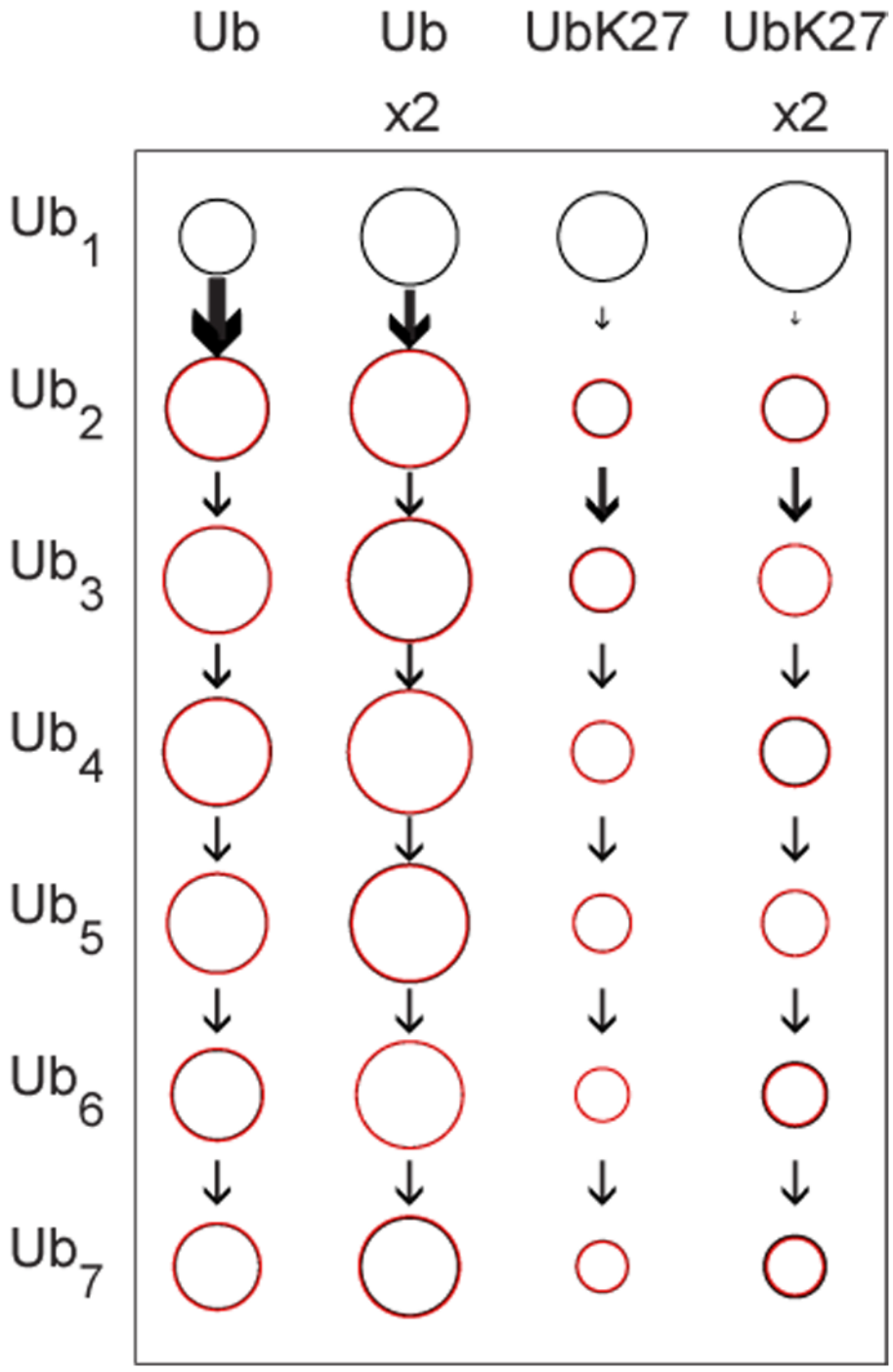

Figure S6. Simulation of the effects of the levels of ubiquitin variants on the stoichiometry of Jun ubiqutination. The relative amounts of ubiquitin conjugates formed by wild type and K27-only ubiquitin expressed at two different levels were simulated based on the amounts of mono-ubiqutinated Jun detected. The only variables unique for each condition were the efficiencies of mono- to di-ubiqutinated Jun conversion. The simulated values (red) were superiposed on the observed amounts (black) displayed as described in Figure 4I.